Calculating S-Parameters and Uncertainties of Coaxial Air-Dielectric Transmission Lines

Ali Mubarak, Faisal; Mascolo, Vincenzo; Hussain, Faizan; Rietveld, Gert

DOI
10.1109/TIM.2023.3338667

Publication date
2024

Document Version
Final published version

Published in
IEEE Transactions on Instrumentation and Measurement

Citation (APA)
Ali Mubarak, F., Mascolo, V., Hussain, F., & Rietveld, G. (2024). Calculating S-Parameters and Uncertainties of Coaxial Air-Dielectric Transmission Lines. *IEEE Transactions on Instrumentation and Measurement*, *73*, 1-11. Article 8000511. https://doi.org/10.1109/TIM.2023.3338667

Calculating *S*-Parameters and Uncertainties of Coaxial Air-Dielectric Transmission Lines

Faisal Ali Mubarak, *Member, IEEE*, Vincenzo Mascolo, Faizan Hussain, and Gert Rietveld, *Senior Member, IEEE*

***Abstract*— Closed-form solutions are presented for calculating the reflection coefficient with corresponding uncertainty of metrology-grade 3.5 mm air-dielectric coaxial transmission lines for use as reference standards in *S*-parameter measurements up to 33 GHz. The closed-form solutions allow the calculation of the sensitivity coefficients required for calculating the propagation of uncertainties from the material and mechanical parameters of the transmission line toward its reflection coefficient uncertainties. The presented uncertainty framework evaluates every uncertainty source's contribution, with uncertainties in reflection coefficient ranging from $1 \cdot 10^{-3}$ up to $6 \cdot 10^{-3}$. The approach is validated up to 33 GHz via a comprehensive measurement comparison of the reflection coefficient parameter for three 3.5 mm transmission lines with 16, 60, and 150 mm lengths. The values obtained by the proposed model agree well within the measurement uncertainties with known traceable calibration results of the transmission lines.**

***Index Terms*— Coaxial transmission line, precision air line, *S*-parameters, vector network analyzer (VNA), VNA traceability.**

I. Introduction

COAXIAL air-dielectric transmission lines are widely used as the basis for traceable *S*-parameter measurements [1], [2], [3], [4], [5]. The characteristic impedance and propagation constant of the transmission line are the principal properties used in vector network analyzer (VNA) calibrations. The measurement accuracy of such line-based calibration methods is fundamentally set by the behavioral model of the transmission line and its ability to account for transmission line imperfections, i.e., the nonuniform diameter of the outer and inner conductors, the losses, the imperfect connectors, and the applied mounting techniques [6], [7], [8]. Taking the uncertainties caused by these error sources correctly into account is of absolute importance for achieving metrology-grade *S*-parameter measurements.

Identifying imperfections of coaxial connectors formed a significant milestone in coaxial *S*-parameter metrology and led to higher accuracy measurements. Several researchers identified connector pin-gap errors and investigated the impact of these errors on *S*-parameter measurements [8], [9], [10]. Advanced mounting methods to control the center conductor position are needed to avoid connector errors with coaxial air-dielectric transmission lines [8].

Over the decades, many works have developed behavior models for estimating transmission line *S*-parameters, interconnecting high-frequency electrical properties to geometrical and material parameters of the transmission line [11], [12], [13]. Here, [11] reported distributed circuit component values for transmission lines with nominal dimensions. However, the method does not directly account for nonideal transmission line properties, so electrical measurements-based techniques were suggested to estimate measurement residuals caused by conductor losses and nonideal connections. This approach is not sufficient for reaching present state-of-the-art *S*-parameter measurement accuracy. In [12], a behavioral model for coaxial transmission lines using generalized telegraphist equations was proposed. An equivalent circuit model accounting for inner conductor eccentricity, diameter variations, and propagation losses was proposed by [13]. The latter also included a sensitivity analysis of the transmission line propagation constant and characteristic impedance for various uncertainty sources. Whereas most behavior models for evaluating *S*-parameters of coaxial air-dielectric transmission lines account for the nonuniform diameter of the outer conductor, inner conductor, and the losses, they have not provided the techniques to account for the connector reflection and mounting effects. This imposes a significant drawback in implementing the aforementioned models and can result in substantial systematic measurement errors. Furthermore, none of the existing behavior models provide a detailed uncertainty framework for the propagation of uncertainties from the identified error sources toward the transmission line *S*-parameters.

This article aims to fill this gap by developing behavioral models of connectors and the transmission line segment, thereby covering all relevant influence factors for transmission line *S*-parameters. The models only require users to provide certain transmission line parameters for calculating the corresponding *S*-parameters and uncertainties up to 33 GHz. The behavioral model is based on closed-form solutions for propagating uncertainties of all relevant parameters of a coaxial transmission line to the corresponding *S*-parameters uncertainty and thus is able to identify the dominant uncertainty contributors. The proposed linear covariance-based uncertainty propagation method is also fully compatible with the widely used software VNA Tools II [14] developed by METAS, the Swiss National Metrology Institute, and the FAME VNA

Manuscript received 25 August 2023; revised 12 October 2023; accepted 8 November 2023. Date of publication 1 December 2023; date of current version 22 December 2023. This work was supported by the Dutch Ministry of Economic Affairs. The Associate Editor coordinating the review process was Dr. Zhengyu Peng. *(Corresponding author: Faisal Ali Mubarak.)*

Faisal Ali Mubarak is with the Electricity and Time Department of VSL, National Metrology Institute of the Netherlands, 2629 JA Delft, The Netherlands, and also with the Electronic Circuits and Architectures (ELCA) Research Group, Delft University of Technology, 2628 CD Delft, The Netherlands (e-mail: fmubarak@vsl.nl).

Vincenzo Mascolo is with European Railway Signaling Company, 80147 Naples, Italy.

Faizan Hussain is with BCube (Pvt.) Ltd., Rawalpindi 46000, Pakistan.

Gert Rietveld is with the Electricity and Time Department of VSL, National Metrology Institute of the Netherlands, 2629 JA Delft, The Netherlands, and also with the Department of EEMCS, University of Twente, 7522 NB Enschede, The Netherlands.

Digital Object Identifier 10.1109/TIM.2023.3338667

software by VSL for evaluating S-parameter measurement uncertainties.

The article is organized as follows. Section II outlines the traceability path for coaxial air-dielectric transmission lines at VSL. Then, Section III describes the proposed behavioral model for the line section of coaxial transmission lines, allowing the computation of the S-parameters and uncertainties of the line section. Section IV details the behavioral model for the coaxial connectors for calculating the S-parameter uncertainty resulting from the connector pin-gap in precision coaxial connectors of pin and socket type. Finally, in Section V, three 3.5 mm transmission lines are used for an extensive measurement comparison up to 33 GHz of the S-parameters and uncertainties are determined using the proposed approach and those from a traceable calibration. This comparison provides a detailed validation of the new approach of coaxial transmission line reflection coefficient S-parameters with uncertainties up to 33 GHz.

II. Path to Traceability

Fig. 1 shows how traceable characterization of 3.5 mm coaxial air-dielectric transmission lines is realized with the proposed behavior models of the line segment and the coaxial connectors of the transmission line. Table I identifies the coaxial transmission line parameters required for traceable evaluation of their characteristic impedance [3], [6], whilst Fig. 1 indicates the techniques for experimentally determining these parameters. Only Table I parameters shown in bold are required to solve the proposed closed-form solutions. The remaining parameters are used to develop the proposed models as described in Sections III and IV. The remainder of this section describes how the values of the different parameters can be determined.

The outer- and inner conductor diameters d_o and d_i are fundamental in calculating the characteristic impedance of a coaxial transmission line [11], [12]. Both are measured along the length of the transmission line with an air gauge measurement system (AGMS) at VSL, a method also employed by [6]. See Section III-C1 for further details. The eccentricity e_i of the center conductor also affects the characteristic impedance of a transmission line and is primarily set by the eccentricity of both test-port connectors e_{TP1} and e_{TP2}. A calibrated microscope combined with an image-based eccentricity measurement (IEM) algorithm estimates the eccentricity parameter, detailed in Section III-C3.

Another major parameter affecting the reflection coefficient is the length of the transmission line. The length of the outer conductor l_o is measured with a 3-D coordinate measuring machine (3DCMM) at VSL, whilst the inner conductor length l_i is measured with coaxial mechanical gauge blocks (MGBs). Both measurement methods are explained in Section III-C2. Subsequently, the transmission line inner conductor recession for both connectors (pin-gaps) pg_1 and pg_2 can be estimated using the measured l_o and l_i values. The mounting method of an air dielectric transmission line deals with controlling the position of the inner conductor at the reference plane position using dedicated Kapton offset disks as demonstrated in [5]. Furthermore, the inner conductor recession of both test-port connectors is also measured with the MGB setup.

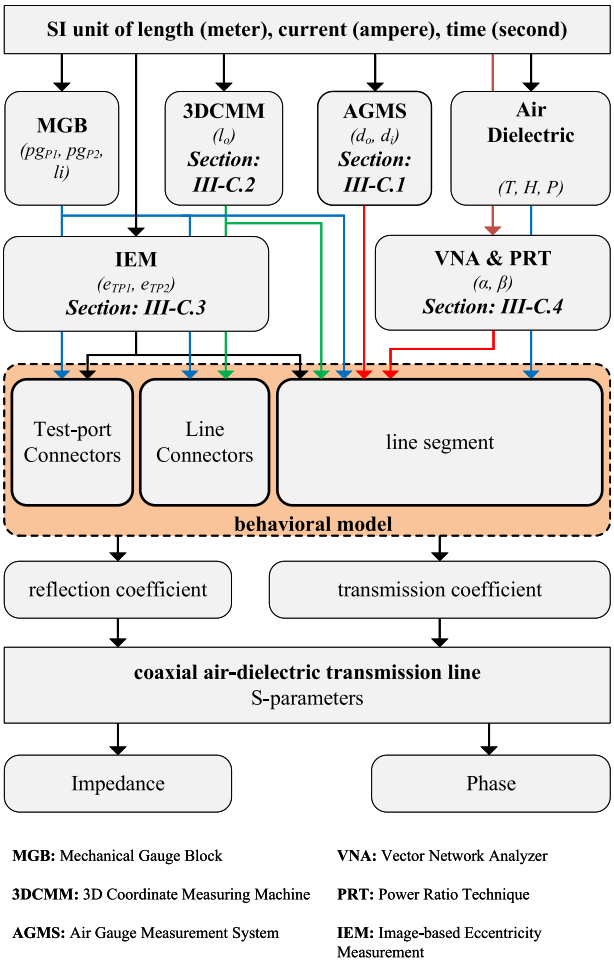

Fig. 1. Traceability chart of 3.5 mm coaxial air dielectric transmission lines at VSL.

Several methods have been developed for characterizing the attenuation and phase constant, also known as the propagation constant, of transmission lines [15], [16], [17]. We estimated the propagation constant by combining results from two independent measurements as in [6]. First, a calibrated VNA measurement provides the broadband transmission parameter of the line. Subsequently, the power ratio technique (PRT) is employed to acquire the transmission line loss at selected frequencies. Whereas the VNA measurement provides broadband data with relatively higher uncertainties, the PRT method delivers better measurement accuracy but at limited frequency points. Combining both measurement results provides sufficient information on the propagation constant for this application.

The metrology-grade transmission lines used at VSL consist of a Beryllium Copper (BeCu) composition with gold plating, and its corresponding conductivity is listed in Table I. Other relevant constants for air dielectric transmission lines are the relative permeability of the air and the permeability of free space. This table also lists the dielectric constants for air and vacuum, where the temperature in the laboratory is maintained at 23 °C. The three metrology-grade coaxial 3.5 mm air-dielectric transmission lines used as validation artifacts are shown in Fig. 2. All three transmission lines undergo traceable characterization of all identified parameters

TABLE I

OVERVIEW OF THE PARAMETERS NEEDED FOR CALCULATING THE *S*-PARAMETERS OF 3.5 MM COAXIAL AIR DIELECTRIC TRANSMISSION LINES. THE FIRST 14 PARAMETERS DENOTED IN BOLD ARE ESTIMATED VIA TRACEABLE MEASUREMENTS AND ARE INPUTS FOR THE PROPOSED MODELS. ALL OTHER PARAMETERS ARE USED FOR THE DEVELOPMENT OF THE PROPOSED BEHAVIORAL MODELS. THE LINE-DEPENDENT PARAMETER VALUES ARE DENOTED WITH LD IN THE THIRD COLUMN

Parameter	Description	Nominal value
$\mathbf{d_i}$ (mm)	center conductor outer diameter	1.52
$\mathbf{d_o}$ (mm)	outer conductor inner diameter	3.50
$\mathbf{e_i}$ (μm)	center conductor eccentricity	0
$\mathbf{l_i}$ (mm)	center conductor length	LD
$\mathbf{l_o}$ (mm)	outer conductor length	LD
$\boldsymbol{\alpha}$	line attenuation constant	LD
$\boldsymbol{\beta}$	line phase constant	LD
$\mathbf{pg_1}$	line connector 1 pin-gap	LD
$\mathbf{pg_2}$	line connector 2 pin-gap	LD
$\mathbf{pg_{P1}}$	test-port 1 connector pin-gap	-
$\mathbf{pg_{P2}}$	test-port 2 connector pin-gap	-
$\mathbf{e_{TP1}}$ (μm)	test-port 1 connector eccentricity	0
$\mathbf{e_{TP2}}$ (μm)	test-port 2 connector eccentricity	0
T	Temperature	23°C
H	Humidity	50%
P	Pressure	1013.25 hPa
ε_0 (F/m)	dielectric constant in vacuum	$8.8542{\cdot}10^{-12}$
ε_r	relative dielectric constant for air at 23 °C, 50 % rel. humidity, 1013.25 hPa atmospheric pressure	1.000649 [3]
μ (H/m)	permeability of free space	$4\pi \cdot 10^{-7}$
μ_r (H/m)	relative permeability for air	1
σ_B (S/m)	conductivity of Berrilium Copper (BeCu)	$1.3{\cdot}10^{7}$ [15]
σ_G (S/m)	conductivity of hard Gold plating	$7.57{\cdot}10^{6}$ [16]
m_i (mm)	pin connector inner chamfer	0.050
m_o (mm)	pin connector outer chamfer	0.020
f_i (mm)	socket connector inner chamfer	0.040
f_o (mm)	socket connector outer chamfer	0.010
h_l (mm)	Pin connector hole length	2.790
d_h (mm)	Pin connector hole diameter	0.960
p_d (mm)	pin diameter	0.927
d_1 (mm)	pin connector inner conductor diameter	1.520
d_2 (mm)	socket connector inner conductor diameter	1.520

to estimate the corresponding *S*-parameters and uncertainties up to 33 GHz.

III. LINE SECTION

The proposed behavior model of the transmission line assumes the line section as a cascade of multiple (N) smaller line segments of 100 μm length as depicted in Fig. 3. Each smaller line segment is considered by a unique two-port *S*-parameter network denoted with $[L]_s$. Consequently, the two-port *S*-parameters of the complete transmission line are determined by cascading the N two-port *S*-parameter networks.

A. Proposed Behavioral Model

This section describes the proposed method for calculating line-section *S*-parameters with corresponding uncertainties. The behavioral response between the line section's reflection coefficient (S_{xx}) and the d_o, d_i, and e_i parameters is investigated through finite-element electromagnetic-field (EM) simulations, an approach widely used in high-frequency

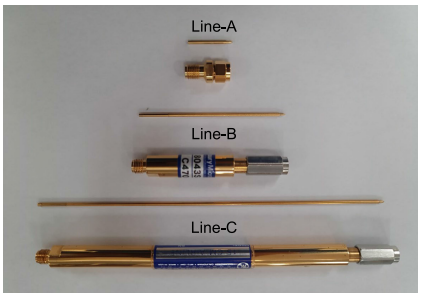

Fig. 2. Photograph of the three metrology-grade 3.5 mm coaxial air-dielectric transmission lines used for validation of the proposed method up to 33 GHz. Here, Line-C and Line-B are 150 and 50 mm in length (manufactured by Maury Microwave), and Line-A is 16 mm in length (manufactured by Keysight Technologies).[1]

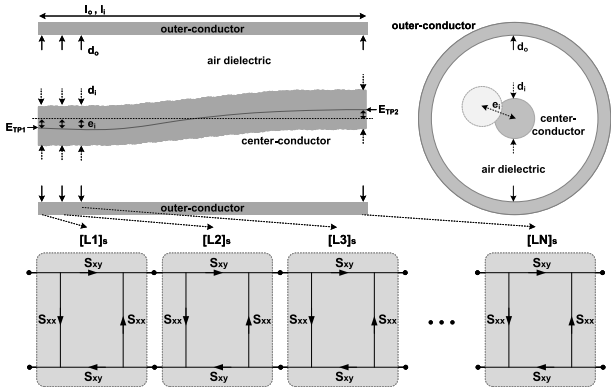

Fig. 3. Transmission line segment as a cascade of multiple (N) smaller line segments of 100 μm length each.

metrology [10]. First, the sensitivity of line sections S_{xx} for each parameter is investigated with EM simulations of a parameterized structure. For this, a 3-D model of a 3.5 mm coaxial transmission line with 100 μm length is designed in CST-microwave studio software and forms the basis for the EM simulations. The offsets for the d_o, d_i, and e_i parameters are sequentially altered from their respective nominal values in steps of 1 μm, ranging between $+50$ and -50 μm. Furthermore, air is used as line dielectric material, and BeCu is used to form the inner and outer conductor of the line section with Gold plating of 1 μm, both with material properties as given in Table I. All EM simulations are conducted using frequency domain solvers for frequencies up to 33 GHz.

Fig. 4 shows a subset of the dataset, providing the sensitivity of S_{xx} for d_o, d_i, and e_i offsets. Subsequently, we calculate the fits for each of the three sensitivity parameters leading to the closed-form equations (1)–(3), depicted with solid lines in Fig 4. The exact values of the polynomial coefficients are provided in Table II.

$$\zeta(d_o, f) = \sum_{v=0}^{1} d_o^v \cdot \sum_{w=0}^{3} k_{w,v} \cdot f^w + \cdots + j \sum_{v=0}^{1} d_o^v \cdot \sum_{w=0}^{3} l_{w,v} \cdot f^w \quad (1)$$

[1]The manufacturers and instrumentation mentioned in this article do not indicate any preference by the authors, nor do they indicate that these are the best available for the application discussed.

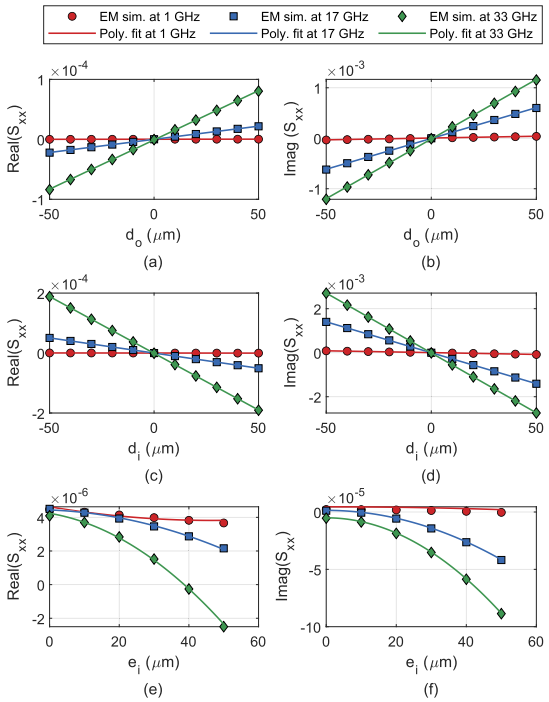

Fig. 4. Simulation results (markers) and polynomial fits (lines) for S_{xx} real and imaginary parts at three different frequencies as a function of (a) and (b) d_o, (c) and (d) d_i, and (e) and (f) e_i offsets from the nominal values listed in Table I.

TABLE II
POLYNOMIAL COEFFICIENTS FOR LINE MODEL

Parameter	$\mathbf{d_i}$	$\mathbf{d_o}$	$\mathbf{e_i}$
$k_{0,0}$	-3.652e-10	1.577e-07	4.645e-06
$k_{1,0}$	1.165e-08	1.155e-08	-1.755e-08
$k_{2,0}$	-8.101e-10	-1.012e-09	4.903e-10
$k_{3,0}$	-1.006e-11	-1.016e-11	-1.003e-11
$k_{0,1}$	-1.655e-09	7.993e-10	-3.841e-08
$k_{1,1}$	-7.093e-10	2.966e-10	3.606e-09
$k_{2,1}$	-3.454e-09	1.499e-09	-1.055e-10
$k_{0,2}$	0	0	4.484e-10
$k_{1,2}$	0	0	-7.264e-11
$l_{0,0}$	4.499e-06	4.5e-06	4.48e-06
$l_{1,0}$	-1.234e-07	-2.237e-07	9.007e-08
$l_{2,0}$	-2.028e-08	-2.026e-08	-2.044e-08
$l_{3,0}$	2.697e-10	2.696e-10	2.711e-10
$l_{0,1}$	1.042e-08	-6.044e-09	1.375e-09
$l_{1,1}$	-1.658e-06	7.199e-07	-1.361e-10
$l_{2,1}$	2.537e-10	-1.096e-10	7.648e-12
$l_{0,2}$	0	0	-1.701e-11
$l_{1,2}$	0	0	-1.012e-09

$$\Delta(d_i, f) = \sum_{v=0}^{1} d_i^v \cdot \sum_{w=0}^{3} k_{w,v} \cdot f^w + \cdots + j \sum_{v=0}^{1} d_i^v \cdot \sum_{w=0}^{3} l_{w,v} \cdot f^w \quad (2)$$

$$\Theta(e_i, f) = \sum_{v=0}^{2} e_i^v \cdot \sum_{w=0}^{3} k_{w,v} \cdot f^w + \cdots + j \sum_{v=0}^{2} e_i^v \cdot \sum_{w=0}^{3} l_{w,v} \cdot f^w. \quad (3)$$

The fitting errors for (1)–(3) are computed and compared with the uncertainty contribution caused by the corresponding parameter offset as detailed in Section V. These are considered to be negligible as the fitting errors are orders of magnitude smaller than the uncertainties due to the d_o, d_i, and e_i offsets.

Using (1)–(3), the reflection coefficient of the transmission line section can be computed as follows:

$$S_{xx}(d_o, d_i, e_i, f) = \zeta(d_o, f) + \Delta(d_i, f) + \Theta(e_i, f). \quad (4)$$

The proposed model is validated by comparing EM simulation and (4) values acquired for various d_o, d_i, and e_i offset configurations. The differences collected from the comparison were negligible compared to the S_{11} uncertainty evaluated in Section V.

The inner conductor offset d_i has the most dominant effect on the line reflection coefficient, about twice as much as the impact of the outer conductor offset d_o, as evident from Fig 4. The sensitivity toward inner conductor eccentricity is hardly noticeable and almost negligible for offsets up to 50 μm, a finding confirmed in [13]. Precision test-port adapters and coaxial transmission lines have inner conductor eccentricity offsets substantially smaller than 50 μm; hence, this uncertainty source can be considered negligible for metrology-grade transmission lines [13].

The propagation constant is directly related to the line section's transmission coefficient (S_{21}). For this reason, the propagation constant is experimentally quantified [3], as described in Section III-C4. For a complete line section, subdivided into N equivalent length smaller lines, the transmission parameter S_{xy} of each section can be calculated as follows:

$$S_{xy} = \sqrt[N]{|\, S_{21} \,|} \cdot e^{j \cdot \angle S_{21}/N}. \quad (5)$$

This approach is beneficial as it accounts for frequency dependence in the attenuation and phase constants. As the section of the line is much shorter than the total line length, the two-port S-parameter network of the section is considered symmetrical ($S_{xx} = S_{11} = S_{22}$ and $S_{xy} = S_{12} = S_{21}$)

$$[L]_s = \begin{bmatrix} S_{xx} & S_{xy} \\ S_{xy} & S_{xx} \end{bmatrix}. \quad (6)$$

With the above, all parameters affecting the characteristic impedance of a coaxial transmission line shown in Table I are interlinked to the corresponding S-parameters. Equations (1)–(6) provide the basis for the S-parameter uncertainty calculation method outlined in Section III-B.

B. Uncertainty Analysis

The proposed method for uncertainty evaluation of the transmission line's S-parameters uses covariance-based uncertainty propagation [18], [19]. The Jacobian matrices necessary for the uncertainty propagation are determined using the closed-form solutions presented in Section III-A. The following steps detail the uncertainty calculation process.

First, the uncertainty assessment corresponding to S_{xx} of a small line segment shown in Fig. 3 is done. As shown in (4), S_{xx} is determined using d_o, d_i, e_i, and frequency parameters. Hence, the uncertainties of d_o, d_i, e_i, and f are grouped in the

covariance matrix Σ_{Li}

$$\Sigma_{Li} = \begin{bmatrix} \sigma_{do}^2 & & & \\ & \sigma_{di}^2 & & \\ & & \sigma_{e_i}^2 & \\ & & & \sigma_f^2 \end{bmatrix}. \tag{7}$$

The partial derivatives necessary for propagation of uncertainties from Σ_{Li} to S_{xx} are grouped in the Jacobian matrix J_L and is calculated based on (4) as follows:

$$J_L = \begin{bmatrix} \frac{\partial \Re(S_{xx})}{\partial(d_o)} & \frac{\partial \Re(S_{xx})}{\partial(d_i)} & \frac{\partial \Re(S_{xx})}{\partial(e_i)} & \frac{\partial \Re(S_{xx})}{\partial(f)} \\ \frac{\partial \Im(S_{xx})}{\partial(d_o)} & \frac{\partial \Im(S_{xx})}{\partial(d_i)} & \frac{\partial \Im(S_{xx})}{\partial(e_i)} & \frac{\partial \Im(S_{xx})}{\partial(f)} \\ \frac{\partial \Re(S_{xy})}{\partial(d_o)} & \frac{\partial \Re(S_{xy})}{\partial(d_i)} & \frac{\partial \Re(S_{xy})}{\partial(e_i)} & \frac{\partial \Re(S_{xy})}{\partial(f)} \\ \vdots & \vdots & \vdots & \vdots \\ \frac{\partial \Im(S_{xx})}{\partial(d_o)} & \frac{\partial \Im(S_{xx})}{\partial(d_i)} & \frac{\partial \Im(S_{xx})}{\partial(e_i)} & \frac{\partial \Im(S_{xx})}{\partial(f)} \end{bmatrix}. \tag{8}$$

The outputs are organized in the following order: $(S_{xx},\ S_{xy},\ S_{xy},\ S_{xx})$. Finally, the covariance matrix Σ_L corresponding to the line segment can be determined with

$$\Sigma_L = J_L \cdot \Sigma_{Li} \cdot J_L^T. \tag{9}$$

The propagation constant is measured for the complete line section. Hence, the corresponding uncertainty is included in the calculation after cascading all smaller line segments. The next objective is to propagate uncertainties of N smaller line segments $\Sigma_{Ln=N}$ to the two-port network of a complete transmission line. It is realized by sequentially propagating uncertainties of two adjacent networks. The cascade C of two adjacent line segments A and B is demonstrated. First, the covariance Σ_{AB} of networks A and B is structured as shown below

$$\Sigma_{AB} = \begin{bmatrix} \Sigma_{L,A} & \\ & \Sigma_{L,B} \end{bmatrix}. \tag{10}$$

Using Σ_{AB}, the covariance Σ_C of the C network is determined using the Jacobian J_{AB}

$$J_{AB} = \begin{bmatrix} \frac{\partial \Re(S_{11C})}{\partial \Re(S_{11A})} & \frac{\partial \Re(S_{11C})}{\partial \Im(S_{11A})} & \cdots & \frac{\partial \Re(S_{11C})}{\partial \Im(S_{22B})} \\ \frac{\partial \Im(S_{11C})}{\partial \Re(S_{11A})} & \frac{\partial \Im(S_{11C})}{\partial \Im(S_{11A})} & \cdots & \frac{\partial \Im(S_{11C})}{\partial \Im(S_{22B})} \\ \vdots & & \ddots & \vdots \\ \frac{\partial \Im(S_{22C})}{\partial \Re(S_{11A})} & \frac{\partial \Im(S_{22C})}{\partial \Im(S_{11A})} & \cdots & \frac{\partial \Im(S_{22C})}{\partial \Im(S_{22B})} \end{bmatrix} \tag{11}$$

whereas the inputs are organized in the following order: $(S_{11A},\ S_{21A},\ S_{12A},\ S_{22A},\ S_{11B},\ S_{21B},\ S_{12B},\ S_{22B})$ and the output variables are structured as follows:

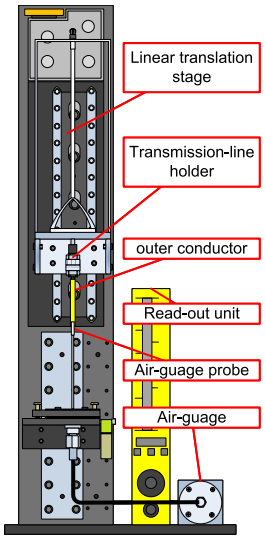

Fig. 5. Overview of the AGMS system to measure the line-section d_o and d_i diameters employing an air-floating top fixture.

$(S_{11C},\ S_{21C},\ S_{12C},\ S_{22C})$. With Σ_{AB} and J_{AB}, the covariance Σ_C of the C network is determined using

$$\Sigma_C = J_{AB} \cdot \Sigma_{AB} \cdot J_{AB}^T. \tag{12}$$

Equations (10)–(12) can be used to propagate uncertainties of N cascaded two-port line segments to form a covariance matrix Σ_L of the complete transmission line.

C. Measurements of Line Section Parameters

1) Measurement of Line Diameters: The line-section d_o and d_i diameters are measured with VSL's AGMS, a measurement technique previously employed in [6]. Fig. 5 shows a system-level overview of the AGMS system at VSL. The top fixture carrying the line outer or inner conductor floats on a so-called air buffer. This method allows the line outer or inner conductor to align accurately with the air gauge probe during the diameter measurement, minimizing the forces in the radial and circumferential axes. Furthermore, a 3DCMM system provides the traceable characterization of the pin and ring reference gauges used to calibrate the AGMS system. As a result, the VSL AGMS system delivers a combined measurement uncertainty of 4 μm with 95% coverage factor. Fig. 6 shows the d_o and d_i measurement results acquired along the length of the transmission lines. The starting position of the measurement, measurement position 0 in Fig. 6, was at the socket connector side of the transmission line. These measurements are conducted for all three coaxial 3.5 mm air-dielectric transmission lines used in this study. A drawback of the AGMS is the inability to measure diameters at both ends of the line sections. Therefore, the line section is mounted with precision adapters at both ends to allow the diameter measurements up to the closest possible vicinity of the line ends. The 3DCMM system provided additional diameter measurements at both ends of the line to validate our approach.

2) Measurement of Transmission Line Length: The length of the line outer conductor is measured with the 3DCMM system, shown in Fig. 7, with a combined measurement uncertainty of 0.5 μm with 95% coverage factor.

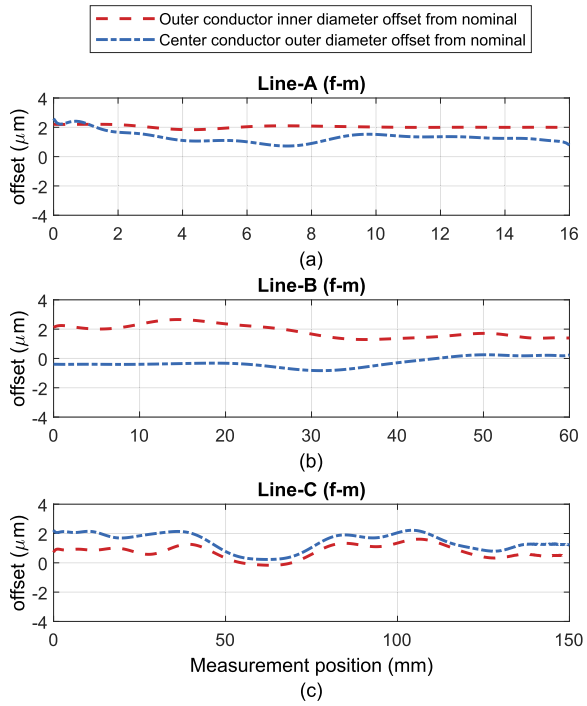

Fig. 6. Outer conductor inner diameter d_o and the center conductor outer diameter d_i measurement offsets from nominal values acquired with the VSL AGMS system for the three coaxial 3.5 mm metrology-grade precision air-dielectric transmission lines, with (a)–(c) depicting results for Line-A, Line-B, and Line-C, respectively. The diameter values are acquired along the length of the transmission line as shown in Fig. 3; measurement position 0 mm is at the socket connector side.

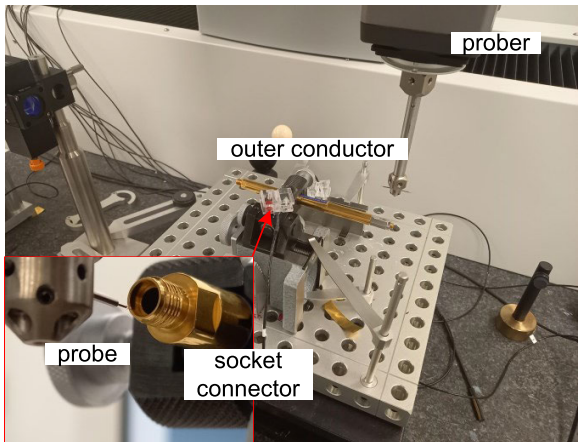

Fig. 7. 3DCMM system at VSL measuring the length of a coaxial 3.5 mm metrology-grade precision air-dielectric transmission line outer conductor.

Once the outer conductor length is known, a mechanical connector gauge gives the inner conductor length by mounting both conductors and using a substitute method. The estimated combined uncertainty of the inner conductor length measurement is less than 2.0 μm. Table III shows the length measurement results for all three coaxial 3.5 mm transmission lines.

3) Measurement of Inner Conductor Eccentricity: The inner conductor eccentricity of test-port connectors primarily determines the line inner conductor eccentricity [6]. An IEM gives eccentricity characteristics for precision coaxial connectors. Here, a calibrated microscope acquires images of the coaxial connector. Subsequently, an image processing algorithm estimates the exact position of the inner and outer conductors,

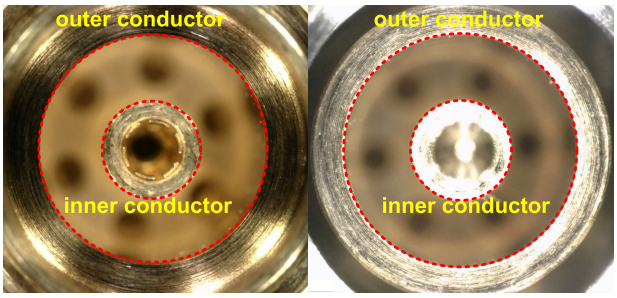

Fig. 8. Top-view images of 3.5 mm coaxial socket (left) and pin (right) type test-port connectors acquired with the IEM system.

providing the inner conductor's eccentricity displacement compared to that of the outer conductor. The expanded uncertainty of this method with a confidence level of 95% is estimated to be 10 μm.

Fig. 8 shows an image of 3.5 mm pin- and socket test-port adapters used for S-parameter measurements at VSL.

4) Measurement of Propagation Constant: Two independent measurement techniques are used to estimate the transmission line propagation constant. The first method characterizes the transmission line propagation constant by measurement of two-port S-parameters. A VNA calibrated with the thru-reflect-line (TRL) method [20] gives a reasonable estimate for the transmission parameter measurements if the transmission line has a sufficiently low reflection at both ports ($\Gamma < 0.010$) [3], [21]. This assumption holds for metrology-grade coaxial air-dielectric transmission lines. Another advantage of this method is that it allows for acquiring measurement data for the entire supported frequency range of the transmission line. However, the disadvantage of TRL-based characterization of the line propagation constant is the significant measurement uncertainty. The combined measurement uncertainty with a coverage factor of 95% for the insertion loss ranges from 0.04 to 0.10 dB. The uncertainty for the phase component is estimated between 0.6° and 1.2° throughout the operational frequency range.

The second method employs the PRT for the measurement of transmission line insertion loss as demonstrated in [22]. Unlike the VNA-based measurement, this method provides measurement only at selective frequencies but with a combined measurement uncertainty of 0.01 dB, which is substantially more accurate than the VNA-based results. Fig. 9 shows the measurement results acquired with both methods for the three coaxial transmission lines used in this study.

IV. Coaxial Connectors

Next to a description of the main line section, a behavior model is needed of the 3.5 mm coaxial connectors terminating the line section, in order to be able to calculate the reflection coefficient and corresponding uncertainty caused by the center conductor recession, more commonly known as the connector pin-gap [9], [23], [24], [25]. The fundamental parameters affecting the reflection coefficient of the pin and socket connectors were identified in [24] and are depicted in Fig. 10. The identified parameters are measured using calibrated microscopes, and the nominal values are summarized in Table I.

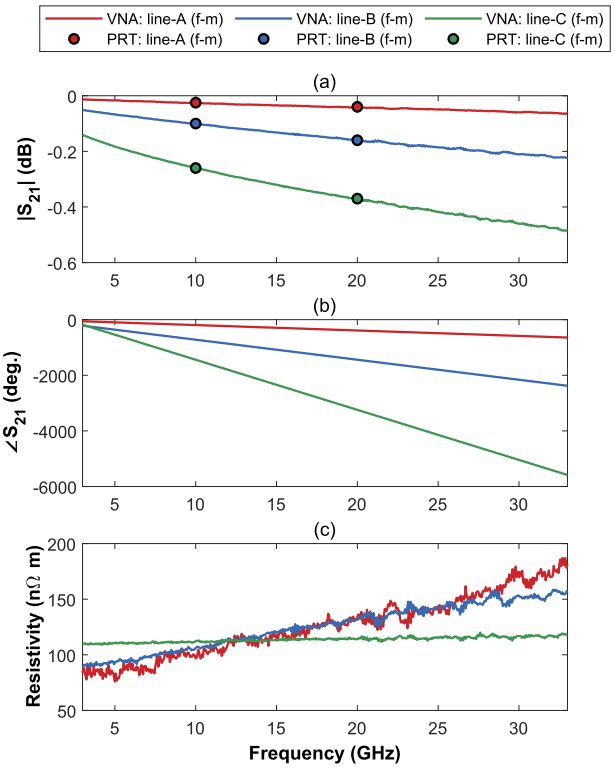

Fig. 9. Measurement results of the propagation constant for the three transmission lines shown in Fig. 2 for respectively (a) attenuation constant and (b) phase constant. (c) Resistivity results for the three transmission lines are acquired with methods outlined in [3].

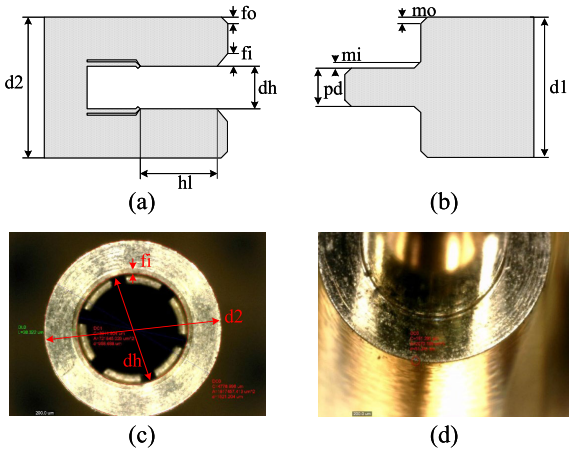

Fig. 10. Parameterization models for 3.5 mm coaxial (a) socket- and (b) pin-type connectors [24]. The parameters are measured with calibrated microscopes, with (c) showing an image of a socket-type connector and (d) depicting a part of a pin-type connector.

A. Behavioral Model

The 3-D model for finite element EM simulations (CST studio software) is designed using the nominal values listed in Table I corresponding to pin- and socket-type connectors. During the simulation exercise, the pin-gap parameter is swept from 0 to 50 μm recession, and the S-parameter datasets were collected.

The CST simulation environment was identical to that used in the transmission line simulations. The dataset provides the sensitivity of the connector reflection coefficient (Γ_{pg}) to the pin-gap value. Subsequently, the fits of the S-parameter

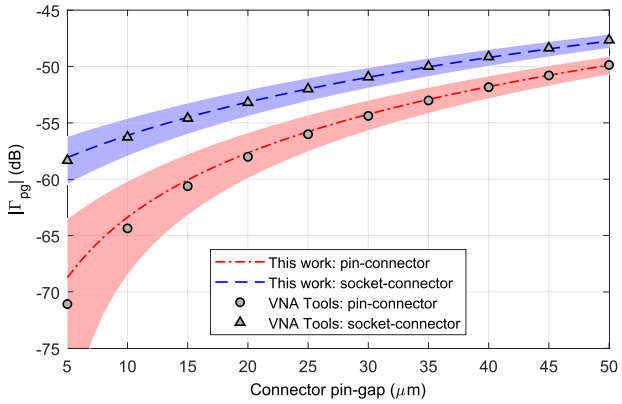

Fig. 11. Comparison of 3.5 mm connector reflection coefficient at 33 GHz caused by connector pin-gap estimated with the METAS VNA II Tools software (markers) and results from the proposed model results (dotted lines). The uncertainty contribution originating from a pin-gap uncertainty of 4 μm is illustrated with colored areas.

results are calculated, leading to the closed-form equation (13). The exact values of the polynomial coefficients for the pin and socket connectors (slotless and slotted) are provided in Table IV

$$\Gamma_{\mathrm{pg}}(\mathrm{pg}, f) = \sum_{v=0}^{1} \mathrm{pg}^v \cdot \sum_{w=0}^{3} m_{w,v} \cdot f^w + \cdots + j \sum_{v=0}^{1} \mathrm{pg}^v \cdot \sum_{w=0}^{3} n_{w,v} \cdot f^w. \tag{13}$$

The transmission coefficient of the pin-gap is determined with the following:

$$S_{xy} = e^{j \cdot \frac{\theta(S_{21}) \cdot \mathrm{pg}}{l_o}}. \tag{14}$$

The two-port S-parameter network of the connector with pin-gap can now be defined with the following:

$$[\mathrm{PG}]_s = \begin{bmatrix} \Gamma_{\mathrm{pg}} & S_{xy} \\ S_{xy} & \Gamma_{\mathrm{pg}} \end{bmatrix}. \tag{15}$$

B. Uncertainty Calculation

To calculate the contribution of the pin-gap to the uncertainty in the transmission line S-parameters, first, the covariance matrix specifying the uncertainty of the pin-gap measurements is determined with

$$\Sigma_{\mathrm{pg}} = \begin{bmatrix} \sigma_{\mathrm{pg}}^2 & \\ & \sigma_f^2 \end{bmatrix}. \tag{16}$$

Then, the Jacobian matrix identifying the relation between the connector reflection coefficient and pin-gap uncertainty is determined via

$$J_{\mathrm{pg}} = \begin{bmatrix} \dfrac{\partial \Re(\Gamma_{\mathrm{pg}})}{\partial \mathrm{pg}} & \dfrac{\partial \Re(\Gamma_{\mathrm{pg}})}{\partial (f)} \\ \dfrac{\partial \Im(\Gamma_{\mathrm{pg}})}{\partial (\mathrm{pg})} & \dfrac{\partial \Im(\Gamma_{\mathrm{pg}})}{\partial (f)} \end{bmatrix}. \tag{17}$$

The Jacobian matrix outputs are organized in the following order (Γ_{pg}, S_{xy}, S_{xy}, Γ_{pg}). Subsequently, the covariance matrix of the connector pin-gap can be calculated with

$$\Sigma_{\mathrm{pg}} = J_{\mathrm{pg}} \cdot \Sigma_{\mathrm{pg}} \cdot J_{\mathrm{pg}}^T. \tag{18}$$

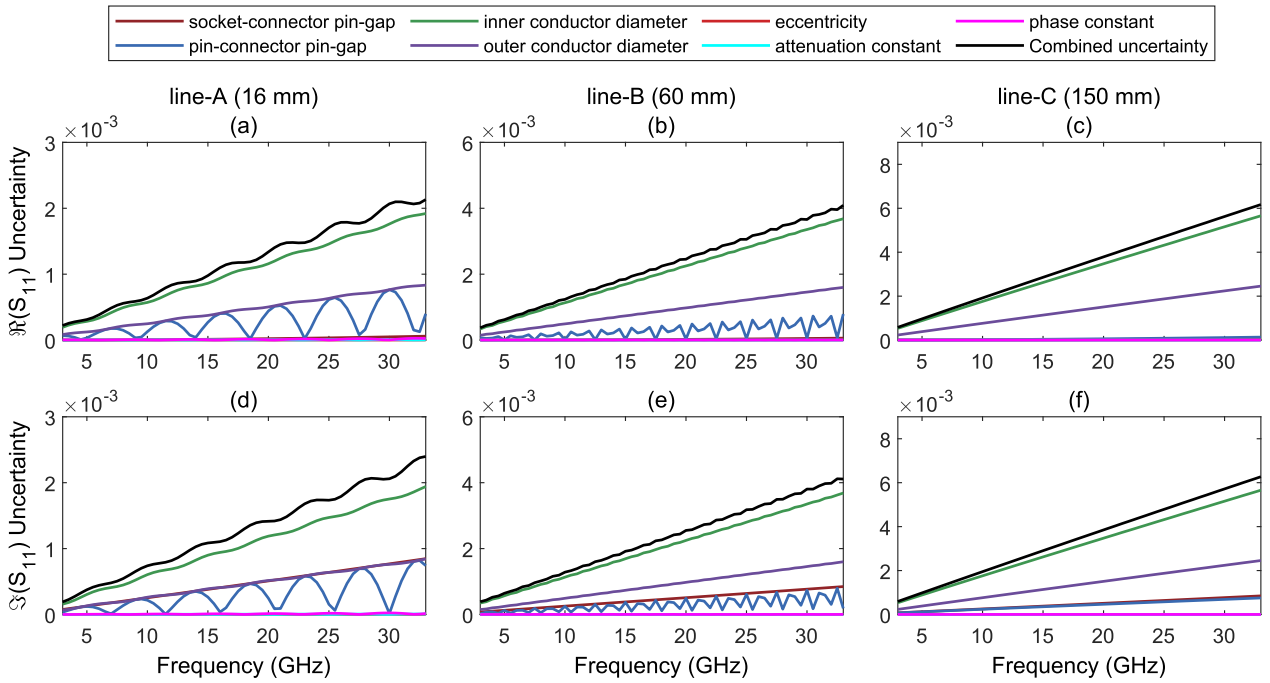

Fig. 12. S_{11} reflection coefficient uncertainty evaluation with the proposed method for the three 3.5 mm coaxial air-dielectric transmission lines used in this study. (a)–(c) Uncertainties corresponding to the real component of S_{11} and (d)–(f) depict the uncertainties corresponding to the imaginary component of S_{11}.

C. Comparison

The connector pin-gap reflection values computed with the proposed closed-form solutions are validated by comparison with the estimates from the METAS VNA tools II software [14]. Fig. 11 shows the resulting reflection coefficients and uncertainties for pin and socket connectors with pin-gap values from 5 to 50 μm, demonstrating a strong agreement of the two approaches, well within the reflection coefficient uncertainty corresponding to a pin-gap uncertainty of 4 μm with 95% coverage factor.

V. Measurement Experiment and Discussion

To validate our approach, the S-parameters and uncertainties evaluated with the proposed methods are compared with traceable measurement results and uncertainties determined using METAS VNA Tools II software.

First, the S-parameters and corresponding uncertainties of the three precision 3.5 mm coaxial air-dielectric transmission lines shown in Fig. 2 are calculated using the proposed method, detailed in Section III-A, with measurement results of all relevant line parameters as detailed in Section III-C. Besides the combined uncertainty contribution accounting for all parameter uncertainties, we also estimate the uncertainty contribution of each uncertainty source individually (see Fig. 12). Here, the uncertainties are estimated for the real and imaginary values corresponding to the port-1 reflection coefficient S_{11}. For brevity, we omit the port-2 (S_{22}) uncertainties as they are comparable to the S_{11} uncertainties.

Subsequently, a Keysight PNA 5225A is used for S-parameter measurements from 3 up to 33 GHz with a 500 MHz step size, with test-port power and IF bandwidth set at -10 dBm and 7 Hz, respectively. Dedicated test-port cables and adapters are combined with VSL-designed test-port fixtures to accurately control test-port cable movements [26]. The port-1 cable was kept fixed during all measurements, while the port-2 cable was moved to minimize RF cable uncertainties.

Before the measurements, the PNA is calibrated using a 3.5 mm precision calibration kit using the SOLT method. The calibration kit reference data are acquired through a traceable calibration by METAS and accounts for connector effects and imperfect test-port adapters [10], [27]. The electrical characteristics of the transmission line are also subject to proper mounting practices. Inaccurate alignment of the center and outer conductor reference planes leads to significant measurement errors [8]. Kapton offset disks are used to accurately position the inner conductors at the correct reference plane to avoid pin-gap errors, a method detailed in [5]. For this, the thickness of the Kapton offset disks is optimized to match the pin-gap of the test-port adapters. The METAS VNA Tools II software computes uncertainties of coaxial S-parameter measurements and uses the METAS UncLib for the linear covariance-based propagation of uncertainties. All uncertainties are linearly propagated through the measurement model, taking correlation into account. The uncertainty analysis accounts for various error sources, including VNA noise and linearity error, drift effects, cable instability, connector repeatability, and calibration standard uncertainties.

The Line-A center conductor length is 7 μm smaller than the outer conductor length, as evident from Table III. The S-parameters of line-A are acquired with a measurement system fit with a 20 μm recessed pin-type test-port adapter on port-1 of the VNA, whereas port-2 is equipped with a socket-type test-port adapter. A Kapton offset disk with 25 μm thickness is mounted on a pin-type test-port adapter, leaving 5 μm recession on the port-1 socket-type connector of line-A. As a result, 2 μm recession remains on the port-2 pin-type connector of line-A. The left column of Fig. 13 shows the S-parameter measurement results of line-A.

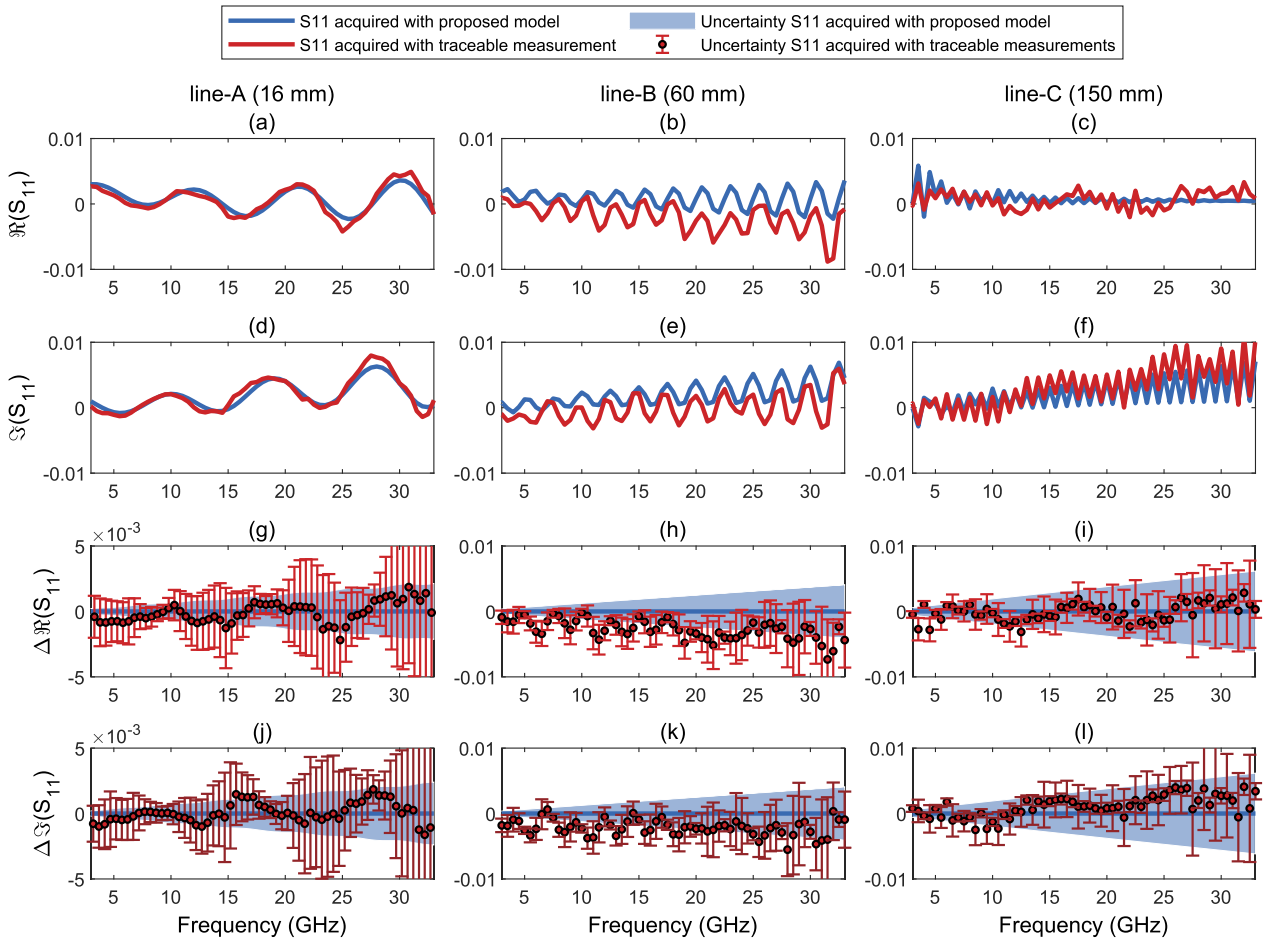

Fig. 13. Measurement results for the three 3.5 mm coaxial air-dielectric transmission lines used in this study. (a)–(c) Real component and (d)–(f) imaginary component of S_{11} measurement results illustrated with red lines and those acquired with the proposed model displayed with blue lines. The differences between the measurement and proposed model results for S_{11} real and imaginary components are shown in (g)–(i) and (j)–(l), respectively. The blue areas indicate the S_{11} uncertainty values with 95% confidence interval estimated with the proposed model, whereas the red bars correspond to the uncertainties with 95% confidence interval computed with VNA tools corresponding to the traceable measurements.

The *S*-parameters of Line-B and Line-C were acquired using a system mounted with a 13 μm recessed socket-type test-port adapter on port-1 of the VNA, whereas port-2 is equipped with a pin-type test-port adapter. Here, a Kapton offset disk with 12.5 μm thickness is mounted on a pin-type connector of both lines, leaving almost zero recession on the port-1 connector of line-B and line-C. As the line-B center conductor length is 3 μm smaller than the outer conductor length (Table III), it leaves a 3 μm recession on the port-2 connector of line-B. The center conductor of Line-C is 4 μm longer than the outer conductor. Hence, when mounted with a 12.5 μm thick offset disk on port-1, it leaves the port-2 center conductor pushing 4 μm into the port-2 test-port connector. We account for this effect by deembedding *S*-parameters of 4 μm recessed pin-type connector on port-2 of Line-C.

Fig. 12 shows the calculated uncertainties using the proposed methods for Line-A, Line-B, and Line-C. The uncertainties for the real and imaginary components of S_{11} corresponding to the port-1 reflection coefficient are shown in Fig. 12. These results show that the center conductor's outer diameter is the most dominant uncertainty contribution, followed by the outer conductor's inner diameter. Subsequently, the uncertainties corresponding to the pin-gaps of port-1 and port-2 connectors are comparable contributors. Other uncertainty sources are much smaller or even negligible, such as the center conductor eccentricity and propagation constant uncertainties. Furthermore, the line length also affects the uncertainty contribution. An increased transmission line length also leads to larger uncertainties, as visible for the combined uncertainties corresponding to Line-A, Line-B, and Line-C.

Finally, Fig. 13 shows the measurement results for Line-A, Line-B, and Line-C. In Fig. 13(a)–(f), the calibration measurement results for the real and imaginary components of S_{11} are depicted with a red line, and those calculated using the proposed method are illustrated with a blue line. The differences between the calibrated measurements and model-based values for the real part of S_{11} are given in Fig. 13(g)–(i), whereas the differences between the measurement and model-based imaginary values of S_{11} are shown in Fig. 13(j)–(l). For brevity, S_{22} results are not included since they are comparable to those of S_{11}. Furthermore, the blue areas shown represent the estimated uncertainty for S_{11} with 95% confidence interval estimated for the model-based values using the techniques outlined in Section III-B. The red bars correspond to the calibrated measurement uncertainties computed with VNA tools and account for calibration standard uncertainties, VNA noise and linearity, connector repeatability, and cable flexure uncertainties.

It is clear from Fig. 13 that the proposed model accurately predicts the S_{11} values, since the differences with the METAS

TABLE III
TRANSMISSION LINE LENGTH MEASUREMENT RESULTS

Parameter	Detail	value (mm)
$l_{i,A}$	Line-A centre conductor length	15.992
$l_{o,A}$	Line-A outer conductor length	15.999
$l_{i,B}$	Line-B centre conductor length	59.914
$l_{o,B}$	Line-B outer conductor length	59.917
$l_{i,C}$	Line-C centre conductor length	149.828
$l_{o,C}$	Line-C outer conductor length	149.824

TABLE IV
POLYNOMIAL COEFFICIENTS FOR PIN GAP MODEL

Parameter	Pin	Socket (slotless)	Socket (slotted)
$m_{0,0}$	5.677e-05	1.789e-05	6.395e-05
$m_{1,0}$	4.513e-06	8.432e-06	1.729e-05
$m_{2,0}$	-2.166e-07	-3.296e-07	2.394e-07
$m_{3,0}$	1.929e-09	4.361e-09	6.857e-09
$m_{0,1}$	2.137e-08	5.527e-08	-2.004e-08
$m_{1,1}$	-3.521e-09	-1.103e-08	-8.866e-10
$m_{2,1}$	8.233e-09	1.393e-08	1.957e-08
$n_{0,0}$	1.354e-06	1.589e-05	3.919e-05
$n_{1,0}$	6.549e-06	9.363e-05	0.0001775
$n_{2,0}$	-3.342e-07	-4.055e-07	-6.854e-07
$n_{3,0}$	5.414e-09	1.587e-08	1.615e-08
$n_{0,1}$	4.364e-07	2.463e-07	1.956e-07
$n_{1,1}$	6.211e-06	6.279e-06	6.645e-06
$n_{2,1}$	7.624e-09	3.939e-09	2.758e-09

measurement results for all three lines are less than the calculated and measurement uncertainties. While the differences for Line-B are also partially within the estimated uncertainties, the results shown in Fig. 13(h) and (k) display some inconsistent behavior, showing the differences for the real and imaginary components of S_{11}.

The estimated uncertainties are also proportional to the frequency, and the comparisons below 5 GHz show larger relative differences compared to frequencies above 5 GHz. Whereas the calculated uncertainties for the proposed model below 5 GHz seem small, the uncertainties corresponding to the measurement results are more considerable as they also account for many error sources residing from the VNA test bench, such as calibration standards, cable movement, and connector repeatability.

The differences between the proposed method and measurement values of *S*-parameters and the estimated uncertainties increase proportionally for longer lines. As the estimated model uncertainties are found in agreement with the behavior of the differences, they illustrate higher confidence in the proposed model's accuracy.

VI. CONCLUSION

Closed-form solutions are derived for calculating the reflection coefficient and uncertainty of precision 3.5 mm coaxial air-dielectric transmission lines up to 33 GHz, based on the material and mechanical parameters of the transmission lines. A main advantage of the proposed approach is its ability to determine the sensitivity coefficients of the uncertainties in the mechanical characterization, needed for propagating these uncertainties into the final reflection coefficient values of the transmission line. A detailed uncertainty evaluation demonstrates that the inner conductor diameter is the most dominant source of uncertainty, followed by the transmission line's outer conductor diameter and connectors. The eccentricity and propagation constant provide a negligible uncertainty contribution to the transmission line's reflection coefficient uncertainty.

To validate the proposed approach, three transmission lines with lengths of 16, 60, and 150 mm were used as verification devices. A comprehensive measurement comparison provides a detailed validation of the transmission line's reflection coefficient parameter up to 33 GHz. The difference between the METAS measurement results and the values obtained by the proposed model are less than the $1 \cdot 10^{-3}$–$6 \cdot 10^{-3}$ uncertainties of the computed reflection coefficients. The validation results clearly prove that the proposed method is suitable for traceable calibration or validation of *S*-parameters at the best accuracy levels.

VII. LIMITATIONS AND FUTURE WORK

The presented method is suitable for 3.5 mm coaxial precision air-dielectric transmission lines with nominal parameters, as listed in Table I. Furthermore, the model is suited for transmission lines with the center conductor and outer conductor diameter offsets smaller than 50 μm, a requirement easily met for metrology-grade transmission lines. This is also evident from d_i and d_o measurement results shown in Fig. 6. The model is unsuitable for transmission lines with fixed center conductors using dielectric beads, as it does not account for dielectric beads, which can result in significant measurement errors.

Our future work aims to extend the proposed model to other coaxial connector interfaces, such as the 7 mm Type-N, 2.92 mm, and 2.4 mm connector interfaces for *S*-parameter measurements up to 50 GHz. Also, a similar approach will be used to develop behavioral models for coaxial short and offset short terminations. Such short terminations together with transmission lines are used as reference standards for traceable *S*-parameter calibration and uncertainty estimation.

REFERENCES

[1] K. H. Wong, "Using precision coaxial air dielectric transmission lines as calibration and verification standards," *Microw. J.*, vol. 31, pp. 83–92, Dec. 1998.

[2] S. Protheroe and N. Ridler, "Using air lines as references for VNA phase measurements," in *ARMMS Conf. Dig.*, Nov. 2005, pp. 1–9.

[3] C. P. Eiø, S. J. Protheroe, and N. M. Ridler, "Characterising beadless air lines as reference artefacts for S-parameter measurements at RF and microwave frequencies," *IEE Proc. Sci., Meas. Technol.*, vol. 153, no. 6, p. 229, 2006.

[4] J. P. Hoffmann, J. Ruefenacht, M. Wollensack, and M. Zeier, "Comparison of 1.85 mm line reflect line and offset short calibration," in *Proc. 76th ARFTG Microw. Meas. Conf.*, Nov. 2010, pp. 1–7.

[5] F. A. Mubarak and G. Rietveld, "Uncertainty evaluation of calibrated vector network analyzers," *IEEE Trans. Microw. Theory Techn.*, vol. 66, no. 2, pp. 1108–1120, Feb. 2018.

[6] M. Horibe, M. Shida, and K. Komiyama, "Development of evaluation techniques for air lines in 3.5- and 1.0-mm line sizes," *IEEE Trans. Instrum. Meas.*, vol. 58, no. 4, pp. 1078–1083, Apr. 2009.

[7] R. Kishikawa, M. Shida, and M. Horibe, "Establishment of S-parameter traceability for 3.5 mm coaxial lines from 10 MHz to 100 MHz," *IEEE Trans. Instrum. Meas.*, vol. 62, no. 6, pp. 1847–1852, Jun. 2013.

[8] F. Mubarak and J. Hoffmann, "Effects of connectors and improper mounting of air lines in TRL calibration," in *Proc. Conf. Precis. Electromagn. Meas. (CPEM)*, Jul. 2016, pp. 1–2.

[9] J. P. Hoffmann, P. Leuchtmann, and R. Vahldieck, "Pin gap investigations for the 1.85 mm coaxial connector," in *Proc. Eur. Microw. Conf.*, 2007, pp. 388–391.

[10] K. Wong and J. Hoffmann, "Improving VNA measurement accuracy by including connector effects in the models of calibration standards," in *Proc. 82nd ARFTG Microw. Meas. Conf.*, Nov. 2013, pp. 1–7.

[11] I. A. Harris and R. E. Spinney, "The realization of high-frequency impedance standards using air-spaced coaxial lines," *IEEE Trans. Instrum. Meas.*, vol. IM-13, no. 4, pp. 265–272, Dec. 1964.
[12] D. R. Holt, "Scattering parameters representing imperfections in precision coaxial air lines," *J. Res. Nat. Bur. Standards*, vol. 94, no. 2, p. 117, Mar. 1989.
[13] P. Leuchtmann and J. Rufenacht, "On the calculation of the electrical properties of precision coaxial lines," *IEEE Trans. Instrum. Meas.*, vol. 53, no. 2, pp. 392–397, Apr. 2004.
[14] M. Wollensack, J. Hoffmann, J. Ruefenacht, and M. Zeier, "VNA Tools II: S-parameter uncertainty calculation," in *Proc. 79th ARFTG Microw. Meas. Conf.*, Jun. 2012, pp. 1–5.
[15] J. R. Juroshek and G. M. Free, "Measurements of the characteristic impedance of coaxial air line standards," *IEEE Trans. Microw. Theory Techn.*, vol. 42, no. 2, pp. 186–191, Feb. 1994.
[16] J. Hoffmann, P. Leuchtmann, J. Ruefenacht, and C. Hafner, "Propagation constant of a coaxial transmission line with rough surfaces," *IEEE Trans. Microw. Theory Techn.*, vol. 57, no. 12, pp. 2914–2922, Dec. 2009.
[17] W. C. Daywitt, "The propagation constant of a lossy coaxial line with a thick outer conductor," *IEEE Trans. Microw. Theory Techn.*, vol. 43, no. 4, pp. 907–911, Apr. 1995.
[18] A. Lewandowski, D. F. Williams, P. D. Hale, J. C. M. Wang, and A. Dienstfrey, "Covariance-based vector-network-analyzer uncertainty analysis for time- and frequency-domain measurements," *IEEE Trans. Microw. Theory Techn.*, vol. 58, no. 7, pp. 1877–1886, Jul. 2010.
[19] M. Garelli and A. Ferrero, "A unified theory for *S*-parameter uncertainty evaluation," *IEEE Trans. Microw. Theory Techn.*, vol. 60, no. 12, pp. 3844–3855, Dec. 2012.
[20] G. F. Engen and C. A. Hoer, "Thru-Reflect-line: An improved technique for calibrating the dual six-port automatic network analyzer," *IEEE Trans. Microw. Theory Techn.*, vol. TT-27, no. 12, pp. 987–993, Dec. 1979.
[21] N. M. Ridler and D. J. Shelton, "Determining the high-frequency resistivity of slightly lossy coaxial air lines," *Metrologia*, vol. 49, no. 6, pp. 644–650, Dec. 2012.
[22] G. F. Engen and R. W. Beatty, "Microwave attenuation measurements with accuracies from 0.0001 to 0.06 decibel over a range of 0.01 to 50 decibel," *J. Res. Nat. Bur. Standard, C Eng. Instrum.*, vol. 64C, no. 2, pp. 139–145, 1960.
[23] B. B. Szendrenyi, "Effects of pin depth in LCP 3.5 mm, 2.4 mm, and 1.0 mm connectors," in *IEEE MTT-S Int. Microw. Symp. Dig.*, vol. 3, Jun. 2000, pp. 1859–1862.
[24] J. P. Hoffmann, P. Leuchtman, J. Ruefenacht, and K. Wong, "S-parameters of slotted and slotless coaxial connectors," in *Proc. 74th ARFTG Microw. Meas. Conf.*, Nov. 2009, pp. 1–5.
[25] Q. C. Zhu and Y. Ji, "Modelling the pin gap effect in coaxial connectors," in *Proc. Conf. Precis. Electromagn. Meas.*, Jul. 2012, pp. 104–105.
[26] F. Mubarak, G. Rietveld, D. Hoogenboom, and M. Spirito, "Characterizing cable flexure effects in S-parameter measurements," in *Proc. 82nd ARFTG Microw. Meas. Conf.*, Nov. 2013, pp. 1–7.
[27] J. Hoffmann, M. Wollensack, J. Ruefenacht, and M. Zeier, "Extended S-parameters for imperfect test ports," *Metrologia*, vol. 52, no. 1, pp. 121–129, Feb. 2015.

Faisal Ali Mubarak (Member, IEEE) received the B.Sc. degree in electrical engineering from the Rijswijk Polytechnic Institute of Technology, Rijswijk, The Netherlands, in 2006, and the M.Sc. degree in electrical engineering from the Delft University of Technology, Delft, The Netherlands, in 2009.

In 2009, he joined VSL, National Measurement Institute, Delft, The Netherlands, where he is currently a Principal Scientist in RF and MW measurements. In 2017, he was one of the Co-Founders of Vertigo Technologies, Delft, a company developing innovative measurement techniques and instruments. His research interests include developing RF measurement systems and techniques up to millimeter-wave frequencies.

Mr. Mubarak is a member of the International Consultative Committee for Electricity and Magnetism Working Group on Radio frequency Quantities and the European Association of National Metrology Institutes technical sub-committee on Radio Frequencies and Microwaves (WG-RF). He is also a member of the IEEE MTT-11 Technical Committee.

Vincenzo Mascolo was born in Naples, Italy, in 1993. He received the B.S. and M.S. (cum laude) degrees in electrical engineering from the University of Naples "Federico II," Naples, in 2015 and 2017, respectively.

In 2017, he completed the M.S. thesis at the Delft University of Technology, Delft, The Netherlands, and VSL, National Measurement Institute, Delft. In 2018, he joined European Railway Signaling Company, Naples, where he currently works as a Work Package Leader. His research interests include mm-wave extreme impedance measurements, electromagnetic imaging, and dielectric spectroscopy techniques.

Faizan Hussain was born in Rawalpindi, Pakistan, in 1995. He received the B.E. and M.S. degrees in electrical engineering from the National University of Sciences & Technology, Islamabad, Pakistan, in 2016 and 2021, respectively.

He completed the M.S. thesis at VSL, National Measurement Institute, Delft, The Netherlands, in September 2020. In 2020, he joined BCube (Pvt.) Ltd., Rawalpindi, where he currently works as a Senior Design Engineer with the Department of RF and Microwave. He has over seven years of industry experience in the RF and microwave domain. His research interests include RF transceivers, active and passive RF circuits, software-defined radio, communication systems, and RF measurement techniques.

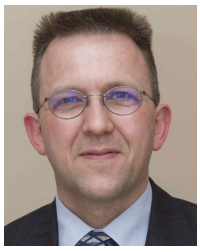

Gert Rietveld (Senior Member, IEEE) received the M.Sc. (cum laude) and Ph.D. degrees in applied physics from the Delft University of Technology, Delft, The Netherlands, in 1988 and 1993, respectively.

Since 1993, he has been with VSL, National Measurement Institute, Delft, where he is currently the Chief Scientist with the Department of Electricity and Time. He has more than 30 years of experience in the area of electrical metrology, with his present work focusing on precision measurements for power and energy and particularly metrology for smart electricity grids. He is also a Full Professor with the University of Twente, Enschede, The Netherlands, where he holds the Chair on "Power and Energy Measurement Systems," working on precision measurements on batteries, measurement of power converter efficiency, and monitoring of electricity grids. He (co)authored more than 250 scientific papers.

Prof. Rietveld is a member of the International Committee for Weights and Measures (CIPM) in Paris and the President of its Consultative Committee for Electricity and Magnetism (CCEM). He is an Active Member of several IEEE, CIGRÉ, CENELEC, and IEC working groups.